

Tuning Crystal Field Potential by Orbital Dilution in Strongly Correlated d^4 Oxides

Wojciech Brzezicki · Filomena Forte · Canio Noce · Mario Cuoco ·
Andrzej M. Oleś

Received: 23 June 2019 / Accepted: 7 November 2019

Abstract We investigate the interplay between Coulomb driven orbital order and octahedral distortions in strongly correlated Mott insulators due to orbital dilution, i.e., doping by metal ions without an orbital degree of freedom. In particular, we focus on layered transition metal oxides and study the effective spin-orbital exchange due to d^3 substitution at d^4 sites. The structure of the d^3 – d^4 spin-orbital coupling between the impurity and the host in the presence of octahedral rotations favors a distinct type of orbital polarization pointing towards the impurity and outside the impurity–host plane. This yields an effective lattice potential that generally competes with that associated with flat octahedra and, in turn, can drive an inversion of the crystal field interaction.

Keywords Spin-orbital order · Octahedral distortions · Orbital dilution · Doped Mott insulator

This work is supported by the Foundation for Polish Science through the IRA Programme co-financed by EU within SG OP Programme.

Wojciech Brzezicki
International Research Centre MagTop, Institute of Physics
PAS, Aleja Lotników 32/46, PL-02668 Warsaw, Poland

Filomena Forte · Canio Noce · Mario Cuoco
CNR-SPIN, IT-84084 Fisciano (SA), Italy;
Dipartimento di Fisica “E. R. Caianiello”,
Università di Salerno, IT-84084 Fisciano (SA), Italy

Andrzej M. Oleś
a.m.oles@fkf.mpg.de
Max Planck Institute for Solid State Research,
Heisenbergstrasse 1, D-70569 Stuttgart, Germany;
Marian Smoluchowski Institute of Physics, Jagiellonian Univ.
Prof. S. Łojasiewicza 11, PL-30348 Kraków, Poland

1 Introduction

Transition metal oxides (TMOs) are fascinating materials where several quantum degrees of freedom (i.e., spin, orbital, charge, lattice) are intertwined, and require to be treated on equal footing both from a fundamental point of view as well as for developing and enhancing applications in the areas of oxide electronics [1]. The competition of different types of ordered states is ubiquitous in strongly correlated TMOs, mainly arising from the complex nature of the spin-charge-orbital couplings where frustrated Coulomb driven exchange competes with the kinetic energy of charge carriers.

A crucial step for accessing the emergent phenomena of correlated TMOs with spin-orbital-charge coupled degrees of freedom is the understanding of the undoped regime [2], where the low-energy physics and spin-orbital order are dictated by effective spin-orbital superexchange [3, 4, 5, 6, 7, 8, 9, 10, 11, 12, 13, 14]. In undoped $3d$ Mott insulators, for instance, large local Coulomb interactions localize electrons and the coupling between transition metal ions is controlled by a low-energy spin-orbital superexchange introduced first by Kugel and Khomskii [4]. When multi-orbital degrees of freedom are included, the enhanced quantum fluctuations for $S = 1/2$ compounds can result in destroying the long range order [5]. On the other hand, spin-orbital entanglement in superexchange models may lead to exotic novel types of magnetic order [15], or stabilize topological order in the ground state and in excited states [16].

Long range order in both spin and orbital sector develops in perovskite lattices when spin fluctuations are weaker for spin S larger than $1/2$. The fate of spin-orbital order is, however, strongly tied to the character of the orbital degrees of freedom that emerges when




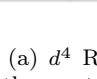
TM ion	configuration	Orbital Polarization and octahedral distortions
Host	$t_{2g}(d^4)$ $\left\{ \begin{array}{l} d_{xz} d_{yz} \uparrow \uparrow \\ d_{xy} \uparrow \downarrow \end{array} \right\}$ $S=1$ $L=1$ <i>doublon</i>	a) $\uparrow \uparrow$ $ c\rangle$  Flat octahedron
		b) $\uparrow \uparrow$ $ b\rangle$  Elongated octahedron
Impurity	$t_{2g}(d^3)$ $\left\{ \begin{array}{l} d_{xz} d_{yz} \uparrow \uparrow \\ d_{xy} \uparrow \end{array} \right\}$ $S=3/2$ $L=0$	c) $\uparrow \uparrow$ $ a\rangle$  Elongated octahedron
		d) $\uparrow \uparrow$ $ a\rangle$  Elongated octahedron

Fig. 1 Artist’s view of the orbital doping when: (a) d^4 Ru ion with spin $S = 1$ and three t_{2g} orbitals split by the crystal field, with $L = 1$ angular momentum, (e) is substituted by the d^3 Cr ion without orbital degree of freedom ($L = 0$) and spin $S = 3/2$ due to Hund’s exchange. Spins are shown by red arrows and doubly occupied t_{2g} orbitals (doublons) are indicated by blue arrows. Depending on the octahedral distortion, the doublon occupies: (b) $|c\rangle$ orbital for a flat octahedron, or (c,d) one of two degenerate doublet $\{|a\rangle, |b\rangle\}$ orbitals for an elongated octahedron.

electrons localize, and on the eventual influence of the atomic spin-orbit coupling. Taking the example of d^4 ions, for large Hund’s exchange high-spin $S = 2$ states emerge at Mn ions in LaMnO_3 [6,17,18,19], and the corresponding A -type antiferromagnetic (A -AF) spin order follows the Goodenough-Kanamori rules [20]. On the other hand, when Hund’s exchange is weaker compared with $t_{2g}-e_g$ splitting, e_g orbitals are empty and intermediate $S = 1$ spin states form at d^4 ions. An example of such a t_{2g} system is Ca_2RuO_4 with spin-orbital superexchange described in section 2. Here, the orbital degree of freedom is set by a doubly occupied orbital configuration called *doublon* [21,22,23], see Figs. 1(b-d), where we introduce the following notation to identify which orbital of the t_{2g} sector is doubly occupied [7],

$$|a\rangle \equiv |yz\rangle, \quad |b\rangle \equiv |xz\rangle, \quad |c\rangle \equiv |xy\rangle. \quad (1)$$

Without distortions, only two out of three t_{2g} orbitals are active along each bond $\langle ij \rangle \parallel \gamma$ and contribute to the intersite kinetic energy, while the third orbital is inactive as the hopping via oxygen is forbidden by symmetry. The inactive t_{2g} orbital along a given cubic axis $\gamma \in \{a, b, c\}$ is in the basis (1) uniquely labeled as $|\gamma\rangle$.

Doping Mott insulators typically refers to the addition of charge carriers that leads to melting of the localized spin-orbital order [24,25] and the formation of metallic states often accompanied by unconventional superconductivity, to novel patterns (stripes, nematic, *etcetera* [26]) of self-organized electronic states [27,28,29], or to the suppression of orbital order by the orbital

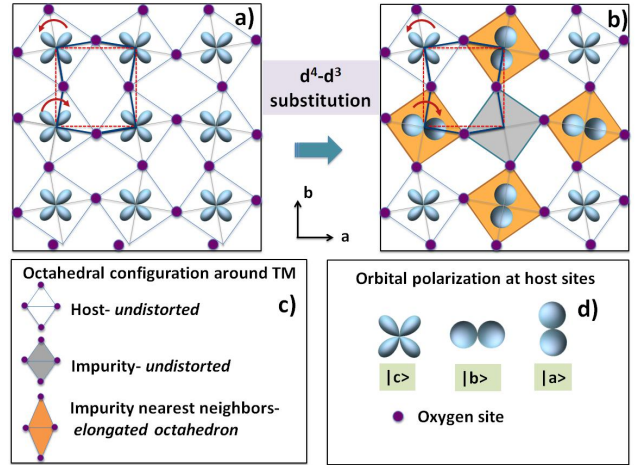


Fig. 2 Artist’s view of the evolution of orbital order from (a) the undoped (a, b) plane of d^4 ions in centers of rotated octahedra (arrows) forming a two-sublattice pattern, (b) the plane with a d^3 ion in the center, and (c) undistorted (elongated) octahedra at (around) the impurity, respectively, shown by gray (orange) color. The undoped state (a) has a uniform ferro-orbital (FO) order with the doublon occupying the $|c\rangle$ orbital. Panel (d) shows the possible orbital configurations (1) of the doublon at an undoped d^4 site, see Fig. 1. Finally, the violet circles stand for oxygen sites in the (a, b) plane.

rotation induced by charge defects [30]. In contrast, substitutional doping of transition metal elements can avoid the breakdown of the Mott insulating state and allows novel directions for tuning the degree of intertwining of the spin-orbital correlations. As an experimental motivation we mention the anomalous magnetic reconstruction that realizes $3d^3$ substitution in a $4d^4$ host, or Mn doping in $\text{Sr}_3\text{Ru}_2\text{O}_7$ [31].

The potential to modify the valence of the transition metal elements without destroying the insulating state also allows to achieve non-standard regimes of competition between lattice and spin-orbital degrees of freedom. Indeed, specific for the present study is the physical case of the Mott insulating Ca_2RuO_4 whose substitution of Ru with Mn [32], Cr [33], Fe [32], or Ir [34] atoms, apart from driving a modification of the spin-orbital order, leads to the observation of negative thermal expansion effects, i.e., the increase of the unit cell volume by thermal cooling. These examples suggest that the negative thermal expansion outcomes are strongly linked to the electronic correlations developing in the doped Mott phase.

The doping path, indeed, makes possible the design of spin-orbital defects that in turn are expected to cause significant deviations from the standard exchange as related to the Goodenough-Kanamori rules [23,35,36,37]. For instance, focusing on a TMO with t_{2g} orbital degrees of freedom, one can achieve orbital dilu-

tion by doping with orbitally inactive transition metal magnetic ions [23]. Such doping of t_{2g} sector can be realized by replacing a d^4 Ru ion with low $S = 1$ spin and effective $L = 1$ angular momentum with a d^3 ion corresponding with a local increase of spin to $S = \frac{3}{2}$ and removal of the orbital degree of freedom (i.e., $L = 0$), see Figs. 1(a) and 1(e). Alternative substitutional doping by d^2 ions employs both the orbital and charge degrees of freedom and is called charge dilution [36, 37].

Focusing on d^3 substitution in d^4 systems, the impurity-host spin-orbital exchange is strongly dependent on the orbital that is doubly occupied in the t_{2g} sector. Indeed, the impurity can act as an orbital vacancy for weak host-impurity coupling or favor an orbital polaronic configuration with the doublon sitting in the active orbitals along the $3d-4d$ bond [23]. For an (a, b) plane, the orbital selection of the doublon configuration couples in a different way to the octahedral distortions corresponding to flat or elongated modes, see Figs. 1(b)–1(d). Thus we explore the interrelation between the orbital order developing around the impurity and the character of the compatible octahedral distortions. We find that the rotation of the octahedra is able to pin uniquely the type of orbital order around the impurity (see Fig. 2). This result indicates a strong bias in the induced octahedral distortions. The main outcomes of the present investigation include:

- (i) the determination of the effective d^3-d^4 superexchange in the presence of octahedral rotations,
- (ii) establishing orbital order around the impurity,
- (iii) providing a discussion on the way the orbital order is linked to the flat or elongated distortions of the octahedra in the host.

2 Spin-orbital superexchange in the host

First we consider the effective spin-orbital superexchange in the host taking the limit of strong local Coulomb interactions U_2 at Ru ions in $4d^4$ local configurations, i.e., charge excitations $d_i^4 d_j^4 \rightarrow d_i^5 d_j^3$, along each bond $\langle ij \rangle$ generate effective superexchange [21, 22, 23],

$$\mathcal{H}_{d^4-d^4} = J_{\text{host}} \sum_{\langle ij \rangle \parallel \gamma} \left\{ \mathcal{J}_{ij}^{(\gamma)} (\mathbf{S}_i \cdot \mathbf{S}_j + 1) + \mathcal{K}_{ij}^{(\gamma)} \right\}. \quad (2)$$

Here superexchange $\propto J_{\text{host}}$ involves spin operators for $S = 1$ spins and includes on the orbital operators, $\mathcal{J}_{ij}^{(\gamma)}$ and $\mathcal{K}_{ij}^{(\gamma)}$, which depend on the orbital doublet active along the bond direction γ ($\langle ij \rangle \parallel \gamma$). The superexchange (2) may be obtained from that for vanadium perovskites with V d^2 ions [38, 39] by electron-hole transformation, where an empty site (holon) transforms into a doublon for d^4 ions. The form of $\{\mathcal{J}_{ij}^{(\gamma)}, \mathcal{K}_{ij}^{(\gamma)}\}$ was given in [38, 39, 40]; J_{host} depends on the hopping t and

on Coulomb U_2 and Hund's exchange J_2^H host parameters, and $\eta_{\text{host}} \equiv J_2^H/U_2$. An additional aspect which we neglect here is that spin-orbital entangled variables that drive magnetism in ruthenates are influenced by electron-lattice coupling, for instance via pseudo-Jahn-Teller effect [41], which focuses on the distortions which split the t_{2g} orbitals.

We consider here a 2D square lattice with transition metal ions connected via oxygen ions as in an (a, b) RuO_2 plane, see Fig. 2, of Ca_2RuO_4 . In this case $|a\rangle$ ($|b\rangle$) orbitals are active along the b (a) axis, while $|c\rangle$ orbitals are active along both a, b axes. Finite crystal field (CF) favors doublons in $|c\rangle$ orbitals, see Fig. 2(a). Below we investigate the effect of orbital dilution shown in Fig. 2(b).

For the host sites we assume AF spin order replacing spin-spin interactions by the correlation function $\langle \mathbf{S}_i \mathbf{S}_j \rangle \simeq -5/4$ (here we neglect spin quantum fluctuations) and add the anisotropic spin-orbit coupling term in a form of,

$$\mathcal{H}_{so} = \lambda \sum_i (-1)^i h_z L_i^z,$$

where h_z is the local staggered magnetic moment assumed to be along z axis and the orbital L_i^z operator has a standard form of $L_i^z = (ia_i^\dagger b_i + H.c.)$. Altogether, the total host Hamiltonian reads, $\mathcal{H}_{\text{host}} = \mathcal{H}_{d^4-d^4} + \mathcal{H}_{so}$.

3 Hybrid bond: Orbital dilution

In this section we present the results of the derivation of effective $3d^3-4d^4$ spin-orbital superexchange as due to the coupling between orbitals of $3d$ and $4d$ ions through the oxygen $2p$ orbitals which build up the $p-d$ hybridization $\propto V_{pd\pi}^2$. For our purposes, it is sufficient to analyze a pair of atoms forming a bond $\langle ij \rangle$, as the effective interactions are generated by charge excitations, $d_i^m d_j^m \rightarrow d_i^{(n+1)} d_j^{(m-1)}$ along a single bond [8]. In contrast to the reference d^4 host where both atoms on the bond $\langle ij \rangle$ are equivalent, a d^3-d^4 hybrid bond has explicitly different ionic configurations. The degenerate Hubbard Hamiltonian $H(i, j)$ [42] includes in general the standard local Coulomb interaction $H_{\text{int}}(i)$ and the effective $d-d$ kinetic term, $H_t(i, j)$; for a representative $3d-2p-4d$ bond after projecting out the oxygen degrees of freedom,

$$H(i, j) = H_t(i, j) + H_{\text{int}}(i) + H_{\text{int}}(j). \quad (3)$$

The case without octahedral rotation was investigated in [23]. Here we present the superexchange Hamiltonian for a bond $\langle 12 \rangle$ along the a axis between the d^3 impurity at site $i = 1$ and a host d^4 ion at site $j = 2$, in presence

of octahedral rotation by angle ϕ ,

$$\begin{aligned} \mathcal{H}_{d^3-d^4}^{(a)}(\phi) &= J_{\text{imp}}(\mathbf{S}_1 \cdot \mathbf{S}_2) \\ &\times \left\{ \alpha_1 + \alpha_2 \left(a_2^\dagger b_2 + b_2^\dagger a_2 \right) + \alpha_3 a_2^\dagger a_2 + \alpha_4 b_2^\dagger b_2 \right\} \\ &+ \left\{ \beta_1 + \beta_2 \left(a_2^\dagger b_2 + b_2^\dagger a_2 \right) + \beta_3 a_2^\dagger a_2 + \beta_4 b_2^\dagger b_2 \right\}. \end{aligned} \quad (4)$$

Here the coefficients $\{\alpha_i\}$ and $\{\beta_i\}$ are given by the Slater-Koster rules [43], with the property that $\{\alpha_2, \alpha_4\}$ and $\{\beta_2, \beta_4\}$ vanish for $\phi = 0$, so they are generated by the rotation. At $\phi = 0$, the Hamiltonian tends to project out the inactive orbital a along the bond $\langle ij \rangle \parallel a$ axis. With angle $\phi \neq 0$, also the c orbital is disfavored so that only the b orbital is the preferred one. In this way we obtain polarization of the orbitals $\{a, b\}$ towards the impurity — the orbital polarizer mechanism, see Fig. 2.

The exact form of the coefficients $\{\alpha_i\}$ and $\{\beta_i\}$ as function of rotation angle ϕ reads as

$$\begin{aligned} \alpha_1 &= -\frac{2}{9}\gamma + \frac{1}{6}q_5 + \frac{4\gamma + 3}{18}q_3, \\ \alpha_2 &= -\sin(2\phi) \left(-\frac{1}{9} - \frac{1}{12}q_5 + \frac{1}{36}q_3 \right), \\ \alpha_3 &= (\sin^2 \phi - \gamma) \left(-\frac{2}{9} - \frac{1}{6}q_5 + \frac{1}{18}q_3 \right), \\ \alpha_4 &= (\cos^2 \phi - \gamma) \left(-\frac{2}{9} - \frac{1}{6}q_5 + \frac{1}{18}q_3 \right), \end{aligned} \quad (5)$$

and

$$\begin{aligned} \beta_1 &= -\frac{2}{3}\gamma - \frac{1}{4}q_5 - \frac{4\gamma + 3}{12}q_3, \\ \beta_2 &= -\sin(2\phi) \left(-\frac{1}{3} + \frac{1}{8}q_5 - \frac{1}{24}q_3 \right), \\ \beta_3 &= (\sin^2 \phi - \gamma) \left(-\frac{2}{3} + \frac{1}{4}q_5 - \frac{1}{12}q_3 \right), \\ \beta_4 &= (\cos^2 \phi - \gamma) \left(-\frac{2}{3} + \frac{1}{4}q_5 - \frac{1}{12}q_3 \right), \end{aligned} \quad (6)$$

with dimensionless parameters,

$$q_i = \frac{1}{i\eta_{\text{imp}} + 1}, \quad \gamma = \left(\frac{t_{c,c}^{(a)}}{\tilde{V}_{pd\pi}^2} \right)^2, \quad \eta_{\text{imp}} = \frac{J_1^H}{\Delta}. \quad (7)$$

The $d^3 - d^4$ superexchange (4), is given by,

$$J_{\text{imp}} = \frac{4\tilde{V}_{pd\pi}^4}{\Delta}, \quad \Delta = I_e + 3(U_1 + U_2) - 4(J_1^H - J_2^H), \quad (8)$$

and is determined by the effective hopping between two neighboring sites in a two-step process $\propto V_{pd\pi}^2$, involving a charge-transfer excitation energy Δ_{CT} along the d - p - d π -bond. We introduce for convenience the energy, $\tilde{V}_{pd\pi}^2 \equiv V_{pd\pi}^2/\Delta_{\text{CT}}$; Coulomb and Hund's exchange parameters are: $\{U_1, J_1^H\}$. The hopping amplitudes are given by the Slater-Koster rules [43],

$$t_{c,c}^{(a)} = -\tilde{V}_{pd\pi}^2 \cos^3(2\phi)$$

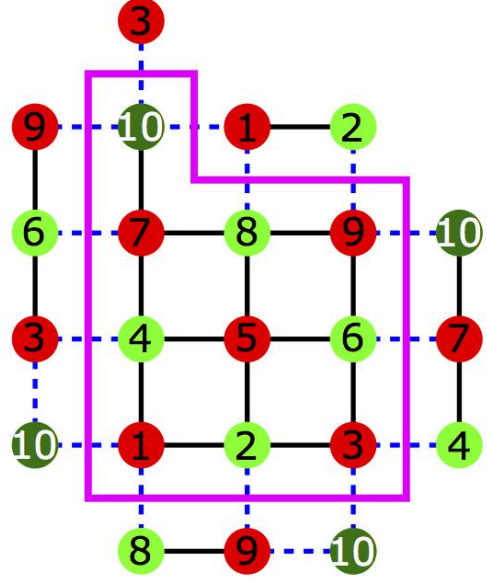


Fig. 3 Schematic view of a 10-site periodic cluster (magenta boarder line) used for calculation of the crystal field at the nearest neighbors of d^3 impurity ($i \in \Omega$, $i = 1, 3, 7, 9$), with impurity at $i = 10$ and $S = \frac{3}{2}$. Orbital degrees of freedom remain undisturbed at next nearest neighbors ($i = 2, 4, 6, 8$) and the only third nearest neighbor $i = 5$ in the cluster. Two-sublattice AF Néel spin order is indicated by green and red sites.

$$+ \frac{1}{8} \left\{ \tilde{V}_{pd\sigma} \left(3\tilde{V}_{pd\sigma} - 4\sqrt{3}\tilde{V}_{pd\pi} \right) \sin(2\phi) \sin(4\phi) \right\}, \quad (9)$$

$$t_{a,a}^{(a)} = \tilde{V}_{pd\pi}^2 \sin^2 \phi, \quad (10)$$

$$t_{b,b}^{(a)} = -\tilde{V}_{pd\pi}^2 \cos^2 \phi, \quad (11)$$

$$t_{a,b}^{(a)} = -\tilde{V}_{pd\pi}^2 \sin \phi \cos \phi. \quad (12)$$

Here we take a realistic assumption, $\tilde{V}_{pd\sigma} = 2\tilde{V}_{pd\pi}$. To obtain the superexchange (4) for a b bond, we transform the coefficients as follows,

$$\alpha_1 \rightarrow \alpha_1, \quad \alpha_2 \rightarrow -\alpha_2, \quad \alpha_3 \rightarrow \alpha_4, \quad \alpha_4 \rightarrow \alpha_3, \quad (13)$$

and analogous for the $\{\beta_i\}$ ones.

4 Results: Crystal field modification

For the exact diagonalization we use a periodic cluster of 10 sites with one impurity at site $i = 10$, see Fig. 3. Since we want to focus on the effect of the impurity, we take it in the strong coupling regime, $J_{\text{imp}} \gg J_{\text{host}}$. We neglect the quantum spin fluctuations and thus the size of the Hilbert space becomes computationally accessible. We consider a collinear AF state described by Ising variables, i.e., we assume the Néel AF spin order. The orbital order in the host is ferro-orbital (FO), with $|c\rangle$ doublons, see Fig. 2(a). The impurity disturbs

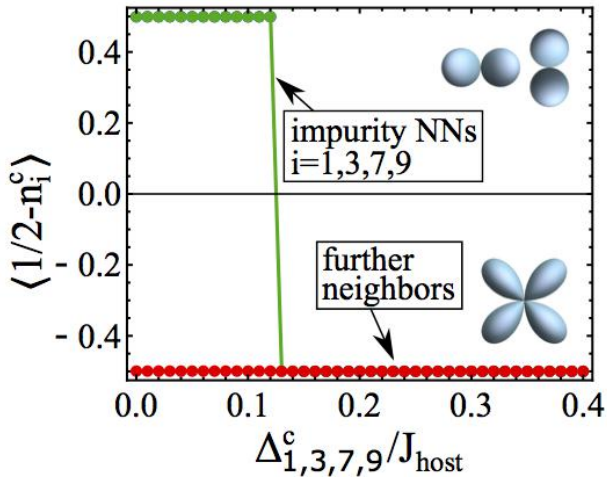


Fig. 4 Occupation of the c orbital at site i of the cluster shown in Fig. 3 as a measure of orbital order for $\phi = 0.25$. The average doublon occupancy $\langle n_i^c \rangle$ changes at site i being a nearest neighbor (NN) of the impurity. For increasing value of the CF splitting at NNs of impurity Δ_i^c , the doublon moves from a directional orbital, a or b , pointing towards the impurity to an in-plane $|c\rangle$ orbital (see insets) and the FO order is restored ($\langle \frac{1}{2} - n_i^c \rangle = \mp \frac{1}{2}$ stands for site i unoccupied/occupied by the c doublon). Energy parameters (all in units of J_{host}): $\lambda = 0.1$, $J_{\text{imp}} = 8.0$; other parameters: $\eta_{\text{host}} = 0.05$, $\eta_{\text{imp}} = 0.2$, $\langle \mathbf{S}_i \cdot \mathbf{S}_{10} \rangle = -2.0$ with $i \in \Omega$.

the orbitals at its neighbors and generates the effective change of the CF due to correlations at the host sites $i \in \Omega$. As a result, for small Δ_i^c the doublons occupy directional orbitals pointing towards the impurity, similar to the orbital polarons in manganites [44, 45, 46].

To estimate the strength of this inverted CF, we put a finite CF Δ_i^c at nearest neighbor sites of the impurity and find that for large enough Δ_i^c the doublon orbital changes from $|a\rangle$ or $|b\rangle$ to $|c\rangle$, i.e., to the one along the bond, see 2(b). The change of orbital occupation at sites around the impurity at $\Delta_i^c \simeq 0.12J_{\text{host}}$ is shown in Fig. 4. Remarkably, the bonds along the a and b axes are equivalent and we observe a change of doublons from directional ($\Delta_i^c \leq 0.12J_{\text{host}}$) to planar ($\Delta_i^c > 0.12J_{\text{host}}$) orbitals. The inversion of CF occurs at the same value of Δ_i^c for the bonds along the a axis ($i = 1, 9$) and along the b axis ($i = 3, 7$), see Fig. 4.

An abrupt change of the doublon orbital is modified to a smooth crossover at finite temperature T , see Fig. 5. Thermal fluctuations generate a rather broad range of CF splitting Δ_1^c , where $\langle \frac{1}{2} - n_1^c \rangle \simeq 0$ and this quantity changes sign close to the value $\Delta_1^c \simeq 0.14J_{\text{host}}$ found before at $T = 0$, see Fig. 4. Interestingly, we find that the strength of the effective CF potential induced by exchange interaction is weakly dependent on temperature, so that such electronically driven orbital splitting is remarkably robust against thermal fluctuations.

5 Discussion and Conclusions

We have shown that orbital doping in the presence of octahedral rotations around the c axis tends to favor a distinct type of orbital order, with orbital polarization that is preferentially directional and distributed both towards the impurity and out-of-plane (i.e., with either xz or yz orbital symmetry). Remarkably, as already demonstrated in the tetragonal symmetric octahedra [23], the pinning of the orbital order can occur for both an antiferromagnetic and ferromagnetic exchange between host and dopants. Its manifestation depends either on the amplitude of Hund's exchange coupling or on the relative strength of the host-host to host-impurity exchange interactions. This means that the local orbital order is a generic sign of the d^3 dopant in a distorted host with octahedral rotations and is robust to spin fluctuations.

Another relevant and striking consequence of the specific orbital order induced locally by the d^3 dopant is that the orbital pattern around the impurity is uniquely compatible with an elongated octahedral configuration, see Fig. 2. Hence, the impurity-host exchange yields an effective crystal field potential that is akin to that obtained when the lattice favors longer out-of-plane transition metal–oxygen bonds than the in-plane ones. On this basis, there are two possible emergent physical scenarios that can occur:

(i) If the lattice potential stabilizes an octahedral configuration that is flat, then, the host-impurity exchange tends to compete with it and, depending on their relative strength, can even end up reversing the sign of the crystal field interaction. This is the case we demonstrate in this paper. Such occurrence clearly implies that the optimal local deformation exhibits an effective enhanced volume of the unit cell due to the bond expansion of the octahedra along the c axis that, in turn, can play a relevant role in setting non-standard negative thermal expansion effects once orbital order is achieved at low temperature.

(ii) On the contrary, for a host configuration with elongated octahedra, the effective host-impurity exchange can enhance the distortions around the impurity thus increasing the stiffness of the lattice. In the present paper, the analysis has been motivated by the study of d^3 dopants in d^4 Mott insulating host with flat octahedra and antiferromagnetic order as it occurs in Mn-doped Ca_2RuO_4 compound [32]. Hence, we speculate that the outcome of the induced elongated octahedra by Coulomb driven orbital exchange may be relevant for the anomalous volume expansion occurring below the onset temperatures of magnetic and orbital order [32].

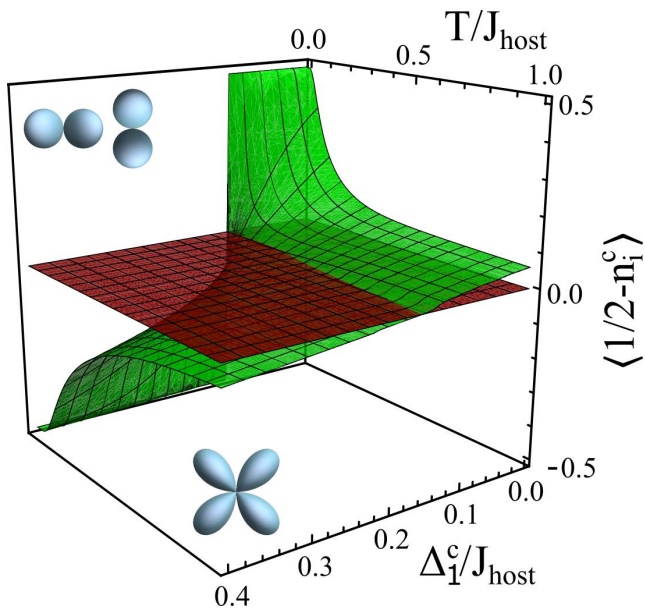


Fig. 5 Evolution of the c orbital occupation at the host site $i = 1$ (green), neighboring with impurity (see Fig. 3), as function of CF Δ_1^c and temperature T [in units of $J_{\text{host}} \equiv 1$]. The average doublon occupancy $\langle n_1^c \rangle$ changes with increasing Δ_1^c or T . The plane (dark red) sets the zero value for the c orbital polarization and separates the regions of a/b doublon ($\langle n_1^c \rangle = 0$) and c doublon ($\langle n_1^c \rangle > 0$). Parameters as in Fig. 4.

It is interesting to point out that similar competing effects between electron correlations and lattice distortions do not occur in transition metal oxides with e_g orbital degrees of freedom, whereas the Jahn-Teller distortions are typically cooperating with the orbital exchange of electronic origin [6, 44, 47, 48]. The local lattice distortions associated with the variation of the orbital order at the metal-insulator transition have been detected by EXAFS and XANES in manganites [49] and recently in PbTiO_3 -based perovskites systems [50]. Therefore, we expect that further experiments will provide interesting information in this field.

We also underline that the temperature dependence of the Coulomb driven effective crystal field (Fig. 5) allows one to have an anomalous thermal behavior when considering the thermal expansion effects. Indeed, since the obtained results show that the amplitude of the effective exchange driven crystal field potential is reduced by the increase of the temperature, then, one can achieve a regime of anomalous volume expansion only in a given window of temperature. This is, for instance, the case of Cr-doped Ca_2RuO_4 [33] where the negative thermal effects manifest predominantly in a range of temperature below the magnetic transition.

Finally, we point out that the proposed reconstruction of the orbital order around the dopant can be accessed by experimental probes based on X-ray spec-

troscopy which is element sensitive and has been successfully demonstrated to unveil the character of the ordered ground state and the corresponding spin-orbital excitations in such transition metal oxides [51, 52].

Acknowledgments Open access funding provided by Max Planck Society. We acknowledge support by Narodowe Centrum Nauki (NCN, National Science Centre, Poland), Project No. 2016/23/B/ST3/00839.

A. M. Oleś is grateful for the Alexander von Humboldt Foundation Fellowship (Humboldt-Forschungspreis).

References

1. Coll, M., Fontcuberta, J., Althammer, M., Bibes, M., Boschker, H., Calleja, A., Cheng, G., Cuoco, M., Dittmann, R., et al.: Towards Oxide Electronics: A Roadmap. *Applied Surface Science* **482**, 1-93 (2019)
2. Khomskii, D.I.: *Transition Metal Compounds*. (Cambridge University Press, Cambridge, 2014)
3. Tokura, Y., Nagaosa, N.: *Orbital Physics in Transition-Metal Oxides*. *Science* **288**, 462-468 (2000).
4. Kugel, K.I., Khomskii, D.I.: The Jahn-Teller effect and magnetism: Transition metal compounds. *Usp. Phys. Nauk* **25**, 621-664 (1982)
5. Feiner, L.F., Oleś, A.M., Zaanen, J.: Quantum Melting of Magnetic Order due to Orbital Fluctuations. *Phys. Rev. Lett.* **78**, 2799-2802 (1997)
6. Feiner, L.F., Oleś, A.M.: Electronic origin of magnetic and orbital ordering in insulating LaMnO_3 . *Phys. Rev. B* **59**, 3295-3298 (2005)
7. Khaliullin, G.: Orbital order and fluctuations in Mott insulators. *Prog. Theor. Phys. Suppl.* **160**, 155-202 (2005)
8. Oleś, A.M., Khaliullin, G., Horsch, P., Feiner, L.F.: Fingerprints of spin-orbital physics in cubic Mott insulators: Magnetic exchange interactions and optical spectral weights. *Phys. Rev. B* **72**, 214431 (2005)
9. Normand, B., Oleś, A.M.: Frustration and entanglement in the t_{2g} spin-orbital model on a triangular lattice: Valence-bond and generalized liquid states. *Phys. Rev. B* **78**, 094427 (2008)
10. Normand, B.: Multicolored quantum dimer models, resonating valence-bond states, color visons, and the triangular-lattice t_{2g} spin-orbital system. *Phys. Rev. B* **83**, 064413 (2011)
11. Chaloupka, J., Oleś, A.M.: Spin-orbital resonating valence bond liquid on a triangular lattice: Evidence from finite-cluster diagonalization. *Phys. Rev. B* **83**, 094406 (2011)
12. Corboz, P., Lajkó, M., Läuchli, A.M., Penc, K., Mila, F.: Spin-orbital quantum liquid on the honeycomb lattice. *Phys. Rev. X* **2**, 041013 (2012)
13. Oleś, A.M.: Fingerprints of spin-orbital entanglement in transition metal oxides. *J. Phys.: Condens. Matter* **24**, 313201 (2012)
14. Brzezicki, W.: Spin, orbital and topological order in models of strongly correlated electrons. arXiv:1904.11772 (2019)
15. Brzezicki, W., Dziarmaga, J., Oleś, A.M.: Noncollinear magnetic order stabilized by entangled spin-orbital fluctuations. *Phys. Rev. Lett.* **109**, 237201 (2012)
16. Brzezicki, W., Dziarmaga, J., Oleś, A.M.: Topological Order in an Entangled $\text{SU}(2) \otimes \text{XY}$ Spin-Orbital Ring. *Phys. Rev. Lett.* **112**, 117204 (2014)

17. Daghofer, M., Oleś, A.M., von der Linden, W.: Orbital Polarons versus Itinerant e_g Electrons in Doped Manganites. *Phys. Rev. B* **70**, 184430 (2004)
18. Kovaleva, N.N., Oleś, A.M., Balbashov, A.M., Maljuk, A., Argyriou, D.N., Khaliullin, G., Keimer, B.: Low-energy Mott-Hubbard excitations in LaMnO_3 probed by optical ellipsometry. *Phys. Rev. B* **81**, 235130 (2010)
19. Snamina, M., Oleś, A.M.: Spin-orbital model of stoichiometric LaMnO_3 with tetragonal distortions. *Phys. Rev. B* **97**, 104417 (2018)
20. Goodenough, J.B.: *Magnetism and the Chemical Bond* (Interscience, New York, 1963)
21. Cuoco, M., Forte, F., Noce, C.: Probing spin-orbital-lattice correlations in $4d^4$ systems. *Phys. Rev. B* **73**, 094428 (2006)
22. Cuoco, M., Forte, F., Noce, C.: Interplay of Coulomb interactions and c -axis octahedra distortions in single-layer ruthenates. *Phys. Rev. B* **74**, 195124 (2006)
23. Brzezicki, W., Oleś, A.M., Cuoco, M.: Spin-orbital order modified by orbital dilution in transition-metal oxides: From spin defects to frustrated spins polarizing host orbitals. *Phys. Rev. X* **5**, 011037 (2015)
24. Lee, P.A., Nagaosa, N., Wen, X.G.: Doping a Mott insulator: Physics of high-temperature superconductivity. *Rev. Mod. Phys.* **78**, 17-85 (2006)
25. Dagotto, E., Hotta, T., Moreo, A.: Colossal Magnetoresistant Materials: The Key Role of Phase Separation. *Phys. Rep.* **344**, 1-153 (2001)
26. Vojta, M.: Lattice symmetry breaking in cuprate superconductors: stripes, nematics, and superconductivity. *Adv. Phys.* **58**, 699-820 (2009)
27. Emery, V.J., Kivelson, S.A., Zachar O.: Spin-gap proximity effect mechanism of high-temperature superconductivity. *Phys. Rev. B* **56**, 6120-6147 (1997)
28. Wróbel, P., Oleś, A.M.: Ferro-Orbitally Ordered Stripes in Systems with Alternating Orbital Order. *Phys. Rev. Lett.* **104**, 206401 (2010)
29. Brzezicki, W., Noce, C., Romano, A., Cuoco, M.: Zigzag and Checkerboard Magnetic Patterns in Orbitally Directional Double-Exchange Systems. *Phys. Rev. Lett.* **114**, 247002 (2015)
30. Avella, A., Oleś, A.M., Horsch, P.: Defect-Induced Orbital Polarization and Collapse of Orbital Order in Doped Vanadium Perovskites. *Phys. Rev. Lett.* **122**, 127206 (2019)
31. Mesa, D., Ye, F., Chi, S., Fernandez-Baca, J.A., Tian, W., Hu, B., Jin, R., Plummer, E.W., Zhang, J.: Single-bilayer E -type antiferromagnetism in Mn-substituted $\text{Sr}_3\text{Ru}_2\text{O}_7$: Neutron scattering study. *Phys. Rev. B* **85**, 180410(R) (2012)
32. Qi, T.F., Korneta, O.B., Parkin, S., Hu, J., Cao, G.: Magnetic and orbital orders coupled to negative thermal expansion in Mott insulators $\text{Ca}_2\text{Ru}_{1-x}\text{M}_x\text{O}_4$ ($\text{M}=\text{Mn}$ and Fe). *Phys. Rev. B* **85**, 165143 (2012)
33. Qi, T.F., Korneta, O.B., Parkin, S., De Long, L.E., Schlottmann, P., Cao, G.: Negative volume thermal expansion via orbital and magnetic orders in $\text{Ca}_2\text{Ru}_{1-x}\text{Cr}_x\text{O}_4$ ($0 < x < 0.13$). *Phys. Rev. Lett.* **105**, 177203 (2010)
34. Yuan, S.J., Terzic, J., Wang, J.C., Li, L., Aswartham, S., Song, W.H., Ye, F., Cao, G.: Evolution of magnetism in single crystal $\text{Ca}_2\text{Ru}_{1-x}\text{Ir}_x\text{O}_4$. *Phys. Rev. B* **92**, 024425 (2015)
35. Brzezicki, W., Cuoco, M., Oleś, A.M.: Novel Spin-Orbital Phases induced by Orbital Dilution. *J. Supercond. Novel Magn.* **29**, 563-568 (2016)
36. Brzezicki, W., Cuoco, M., Oleś, A.M.: Exotic Spin-Orbital Physics in Hybrid Oxides. *J. Supercond. Novel Magn.* **30**, 129-134 (2017)
37. Brzezicki, W., Cuoco, M., Forte, F., Oleś, A.M.: Topological Phases Emerging from Spin-Orbital Physics. *J. Supercond. Novel Magn.* **31**, 639-645 (2018)
38. Khaliullin, G., Horsch, P., Oleś, A.M.: Spin Order due to Orbital Fluctuations: Cubic Vanadates. *Phys. Rev. Lett.* **86**, 3879-3882 (2001); Theory of Optical Spectral Weights in Mott Insulators with Orbital Degrees of Freedom. *Phys. Rev. B* **70**, 195103 (2004)
39. Oleś, A.M., Horsch, P., Khaliullin, G.: One-dimensional Orbital Fluctuations and the Exotic Magnetic Properties of YVO_3 . *Phys. Rev. B* **75**, 184434 (2007)
40. Horsch, P., Oleś, A.M., Feiner, L.F., Khaliullin, G.: Evolution of Spin-Orbital-Lattice Coupling in the $R\text{VO}_3$ Perovskites. *Phys. Rev. Lett.* **100**, 167205 (2008)
41. Liu, H., Khaliullin, G.: Pseudo-Jahn-Teller Effect and Magnetoelastic Coupling in Spin-Orbit Mott Insulators. *Phys. Rev. Lett.* **122**, 057203 (2019)
42. Oleś, A.M.: Antiferromagnetism and Correlation of Electrons in Transition Metals. *Phys. Rev. B* **28**, 327-339 (1983)
43. Slater, J.C., Koster, G.F.: Simplified LCAO Method for the Periodic Potential Problem. *Phys. Rev.* **94**, 1498-1524 (1954)
44. Kilian, R., Khaliullin, G.: Orbital polarons in the metal-insulator transition of manganites. *Phys. Rev. B* **60**, 13458-13469 (1999)
45. Van Aken, B.B., Jurchescu, O.D., Meetsma, A., Tomioka, Y., Tokura, Y., Palstra, T.T.M.: Orbital-Order-Induced Metal-Insulator Transition in $\text{La}_{1-x}\text{Ca}_x\text{MnO}_3$. *Phys. Rev. Lett.* **90**, 066403 (2003)
46. Geck, J., Wochner, P., Kiele, S., Klingeler, R., Reutler, P., Revcolevschi, A., Büchner, B.: Orbital Polaron Lattice Formation in Lightly Doped $\text{La}_{1-x}\text{Sr}_x\text{MnO}_3$. *Phys. Rev. Lett.* **95**, 236401 (2005)
47. Okamoto, S., Ishihara, S., Maekawa, S.: Orbital ordering in LaMnO_3 : Electron-electron and electron-lattice interactions. *Phys. Rev. B* **65**, 144403 (2002)
48. Cuoco, M., Noce, C., Oleś, A.M.: Origin of the optical gap in half-doped manganites. *Phys. Rev. B* **66**, 094427 (2002)
49. Lanzara, A., Saini, N.L., Brunelli, M., Natali, F., Bianconi, A., Radaelli, P.G., Cheong, S.-W.: Crossover from large to small polarons across the metal-insulator transition in manganites. *Phys. Rev. Lett.* **81**, 878 (1998)
50. Pan, Z., Chen, J., Yu, R., Patra, L., Ravindran, P., Sanson, A., Milazzo, R., Carnera, A., Hu, L., Yamamoto, H., et al.: Giant Negative Thermal Expansion Induced by the Synergistic Effects of Ferroelectrostriction and Spin-Crossover in PbTiO_3 -Based Perovskites. [arXiv:1902.04757](https://arxiv.org/abs/1902.04757) (2019)
51. Das, L., Forte, F., Fittipaldi, R., Fatuzzo, C.G., Granata, V., Ivashko, O., Horio, M., Schindler, F., Dantz, M., Tseng, Yi, et al.: Spin-orbital excitations in Ca_2RuO_4 revealed by resonant inelastic X-ray scattering. *Phys. Rev. X* **8**, 011048 (2018)
52. Porter, D.G., Granata, V., Forte, F., Di Matteo, S., Cuoco, M., Fittipaldi, F., Vecchione, A., Bombardi, A.: Magnetic anisotropy and orbital ordering in Ca_2RuO_4 . *Phys. Rev. B* **98**, 125142 (2018)